Comparison of the post-liquefaction behaviour of hard-grained and crushable pumice sands

R P Orense, M S Asadi
Department of Civil & Environmental Engineering, University of Auckland, NZ
r.orense@auckland.ac.nz (Corresponding author)

M Rouholamin
School of Civil Engineering and Surveying, University of Portsmouth, UK

S. Bhattacharya
Department of Civil and Environmental Engineering, University of Surrey, UK

Keywords: earthquake, post-liquefaction, hard-grained sands, crushable sands, triaxial test

ABSTRACT

While the factors affecting the liquefaction resistance of sands have been studied by many researchers, their behaviour post liquefaction needs further examination. More specifically, understanding the effects of various parameters on the stress-strain relation of sands during the post-liquefaction stage is important not only for the purpose of assessing the magnitude of ground deformations induced by liquefaction, but also in investigating the impact of these deformations on buried structures, such as pipelines and pile foundations. In this paper, the post-liquefaction stress-strain behaviour of both hard-grained (silica) and crushable (pumice) sands is examined and attempts are made to express the stress-strain relation using a bilinear model which can be defined in terms of three parameters: initial shear modulus (G_1), shear modulus at recovery (G_2), and dilation shear strain (γ_{dil}) when the soil starts to dilate during post-liquefaction state. For hard-grained sands, it is observed that the three parameters are dependent on the initial relative density (D_r), i.e. with the increase in D_r, G_1 and G_2 would increase while γ_{dil} would decrease. On the other hand, test results on pumiceous sand show that, regardless of D_r, the value of $G_1$is larger while that of G_2 and γ_{dil} are smaller compared to those of a hard-grained sand. This can be attributed, partly at least, to crushing of the particles and their high angularity which induce interlocking between them when monotonically sheared.

1 INTRODUCTION

Past severe earthquakes have shown that failures and large flow slides happened after the cessation of shaking (e.g., Seed et al., 1975; Hamada, 1992). These deformations are typically triggered by earthquakes in liquefiable saturated sandy soils near river banks and quay walls, when horizontal ground movements and lateral spreading occurred after being subjected to seismic shaking. They can also be initiated in slopes and embankments where initial driving shear stresses existed. Such delayed failures and large ground movements are actually the result of a drastic reduction or even complete loss in the shear strength of saturated sand.

One of the key information required to estimate earthquake-induced displacement is the post-liquefaction stress-strain response of sand. Specifically, sand response, when it undergoes movements under states of zero effective stress, is needed when modeling the spatial effect of liquefaction underneath a given structure. In addition to estimating the magnitude of liquefaction-induced ground movements (lateral spreading, settlements and other associated ground deformations), post-liquefaction stress-strain response of sand is also required in estimating the *p-y* curve for analysing soil-structure interaction (i.e. using Winkler method).

However, there is a little research done to date in terms of understanding the post-liquefaction response of sand. Yasuda et al. (1995) carried out a series of multi-stage soil element tests on Toyoura sand at different relative densities. Vaid and Thomas (1995) carried out a similar test procedure on Fraser River sand with different relative densities and effective confining stress. In these works, the soil samples were made to liquefy first by applying cyclic loading followed by monotonic shearing under a certain constant strain rate. The results indicated that the liquefied sand showed nearly zero stiffness up to a particular level of strain, after which the soil resistance increased dramatically with strain. Focusing on the effect of axial strain, relative density and effective confining pressure on the post-liquefaction behaviour of sands, Sitharam et al. (2009) carried out cyclic triaxial tests on Ahmadabad sand (India) while Shamoto et al. (1997), Hyodo et al. (1998), and Kokusho et al. (2004) carried out similar studies. The main conclusion is that the undrained stress-strain response of post-liquefaction sand is dependent on the relative density of the sand while the effect of initial confining pressure is insignificant. However, no attempt has been made to incorporate this into a stress-strain model for liquefied sand.

The post-liquefaction stress-strain behaviour of sandy soils is generally of interest; however, that of other local soils, such as the highly crushable pumiceous sands (in the North Island of New Zealand) need to be equally addressed because many engineering projects are constructed in areas underlain by these deposits. A question that arises is whether the post-liquefaction stress-strain behaviour of crushable pumiceous soils is similar to those of hard-grained sands.

This paper presents the results of two independent but similar researches: (1) Phase 1 involved a series of multi-stage cyclic triaxial tests on different hard-grained sandy soils – two commercially available sands and two natural sands; and (2) Phase 2 comprised multi-stage cyclic triaxial tests on crushable natural pumiceous sands and hard-grained Toyoura sand. These tests were conducted with the aim of investigating the effect of relative density on the post-liquefaction stress-strain behaviour of both hard-grained and crushable soils.

2 MATERIALS AND EXPERIMENTAL METHOD

2.1 Phase 1 sand samples

Phase 1 of the research was conducted at SAGE (Surrey Advanced Geotechnical Engineering) Laboratory at the University of Surrey, U.K. Four types of sand were used to carry out the experimental investigation; two commercially available sands, Redhill-110 sand (UK) and Silica sand No. 8 (Japan), which are typically used in laboratory studies; and two natural sands from India, Assam sand and Ganga sand. Table 1 lists their index properties based on ASTM standards while Figure 1(a) shows their grain size distribution curves. Note that all four sands have uniform grain size distribution and low fines content. Also indicated in the figure is the range of grain size distributions of sands which are deemed to be liquefiable or highly liquefiable, as stipulated in the port and harbour facilities design code (PHRI, 1997).

2.2 Phase 2 sand samples

Phase 2 of the research was performed at the Geomechanics Laboratory of the University of Auckland. The materials used were natural pumiceous soils obtained from three different sites in the Waikato basin; these are referred to herein as NP1, NP2 and NP3 samples and obtained at depths of 1.5m, 2m and 4.5m, respectively, using block sampling. Details of the locations are discussed by Asadi et al. (2017). For the purpose of comparison, another set of tests was performed on Toyoura sand, known as hard-grained, sub-angular material and commonly used in Japan. The Japanese standard method was followed to measure the index properties of the materials and the results are also summarised in Table 1. The corresponding grain size distribution curves are shown in Figure 1(b). The Scanning Electron Microscope (SEM) images of pumice and Toyoura sands are illustrated in Figure 2 where the distinct feature of pumice can be clearly distinguished.

Table 1: Index properties of the materials used

	Sand name	Specific gravity, G_s	Mean diameter, D_{50} (mm)	Maximum void ratio, e_{max}	Minimum void ratio, e_{min}
Phase 1	Redhill-110 (UK)	2.65	0.18	1.04	0.61
	Silica sand No. 8 (Japan)	2.65	0.16	1.38	0.80
	Assam sand (India)	2.68	0.30	0.96	0.62
	Ganga sand (India)	2.67	0.35	1.00	0.85
Phase 2	NP1 (NZ)	2.53	0.60	0.99	0.65
	NP2 (NZ)	2.50	0.17	1.33	0.82
	NP3 (NZ)	2.54	0.24	1.74	1.04
	Toyoura sand (Japan)	2.66	0.21	0.89	0.61

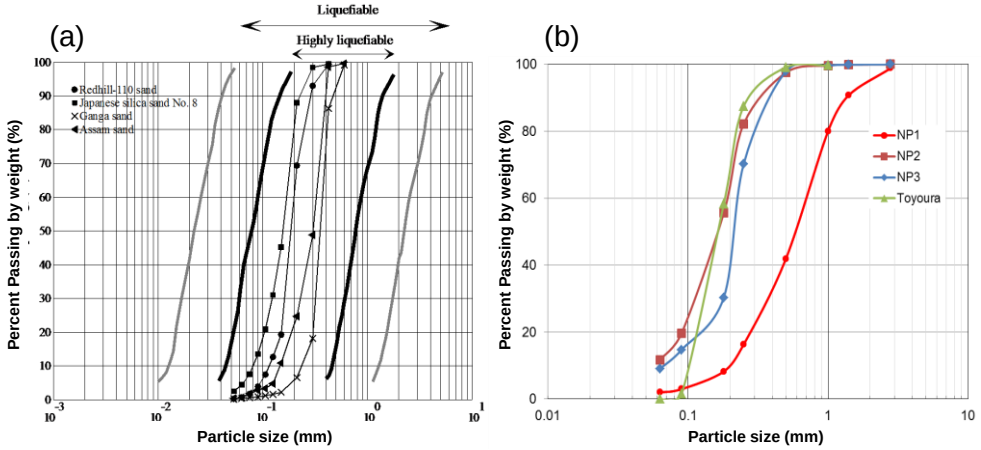

Figure 1: Particle size distribution curves: (a) Phase 1 materials; (b) Phase 2 materials.

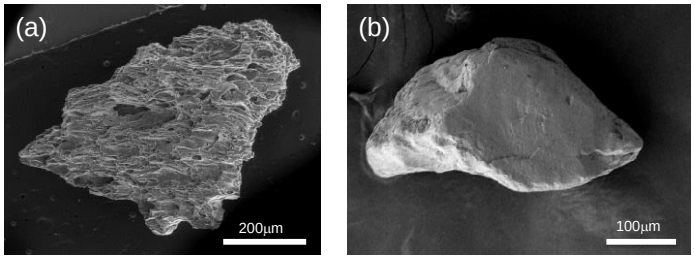

Figure 2: SEM images of particles: (a) pumice sand; (b) Toyoura sand.

2.3 Multi-stage undrained triaxial tests

In both phases of the research, several series of advanced soil testing (i.e. multi-stage soil element test) using cyclic triaxial apparatus were performed. In Phase 1, the 100mm diameter and 200mm high specimens were prepared using the dry pluviation method. In Phase 2, moist tamping was used to avoid segregation of the lighter pumiceous materials during preparation of the 63mm diameter and 126mm high specimens. The specimens were saturated with high back pressure, resulting in B-values in excess of 0.95. They were then isotropically consolidated in order to obtain the target effective confining pressure (σ'_c). Undrained stress-controlled sinusoidal cyclic loading with frequency of 0.1Hz was initially applied in order to liquefy the soil sample, with the amplitude of the cyclic load varied for the cases investigated. This cyclic load was stopped when the onset of liquefaction was recorded. In Phase 1, the onset of liquefaction was considered as the condition of: (a) zero effective stress for loose to medium dense condition, and (b) development of 5% double amplitude axial strain for dense condition. The latter was considered in all tests in Phase 2. Once the specimen liquefied, strain-controlled monotonic load was then applied under undrained condition to obtain the stress-strain curve of the liquefied sand keeping the drainage valve closed. The monotonic load was applied at a rate of 0.1% axial strain per minute. Such

multi-stage tests were conducted under different conditions of initial relative densities (D_r=30-80%), effective confining pressure (σ'_c=50-150 kPa), and applied cyclic deviator stress (σ_d=20-50 kPa) in order to have different levels of Cyclic Stress Ratio (*CSR*).

3 RESULTS AND DISCUSSION

3.1 Phase 1

Typical results of the undrained cyclic triaxial tests are shown in Figure 3. Figure 3(a) corresponds to those for medium-dense Redhill-110 sand samples (D_r=50%) which was isotropically consolidated under σ'_c=100 kPa and cyclically sheared with σ_d=30 kPa. As seen from the figure, the development of axial strain in the sample is slow during the early part of cyclic loading; then large axial strain is mobilised and the sample liquefied at nearly 10 cycles. With the generation of the excess pore water pressure, the effective stress decreases; consequently, the axial strain in the soil increases. Figure 3(b) displays the results for medium dense Assam sand under similar initial effective confining pressure and amplitude of cyclic deviator stress. The sand liquefied after around 23 cycles with the development of 5% double amplitude axial strain. The condition of momentary zero effective stress was also observed.

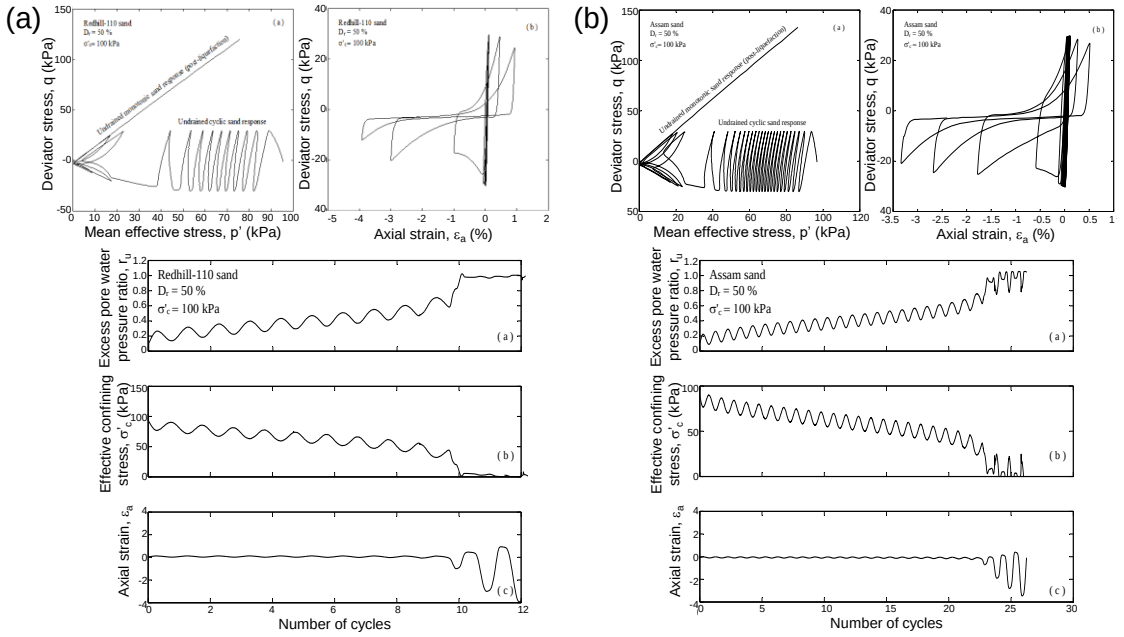

Figure 3: Typical results of the cyclic stage in Phase 1: (a) Redhill-110 sand; and (b) Assam sand.

Figure 4 shows the post-liquefaction response of two types of sands for the same level of *CSR*, in terms of variation of deviator stress and excess pore water pressure ratio with axial strain. From the figures, it can be seen that when the undrained monotonic load is applied to a liquefied specimen, it shows very small stiffness at the beginning of the loading until a certain level of axial strain is reached. After that, the resistance increases dramatically due to dilatancy induced by particle rearrangement. From the test results, it was observed that the axial strain at which such increase in resistance occurs depends on the initial density of the sand. Details of the results for the other sands are discussed by Rouholamin et al. (2017).

Looking at a typical deviator stress-axial strain curve post liquefaction, depicted in Figure 5(a), it is observed that the stiffness of the sand is almost negligible during the initial stage of monotonic loading; with continuous straining, the strength is recovered when a certain level of axial strain is reached. For better understanding of the response, the axial strain-deviator stress curve is

converted to a shear strain-shear stress curve (see Figure 5(b)). Essentially, it can be seen that the shear stress-shear strain curve can be modelled as bilinear, and represented by three parameters: the slope G_1 corresponding to the initial shear modulus (i.e. at the beginning of the loading); the slope G_2, representing the shear modulus during recovery stage; and γ_{dil}, the shear strain when the excess pore water pressure starts to significantly decrease (or when the shear stress increases remarkably) due to dilatancy. In this paper, the shear strain γ_{dil} is determined as the intersection of two tangent lines in the excess pore water pressure ratio versus shear strain curve (see Figure 5(f)). From the results of tests on all four types of sands, it would appear that each of these parameters is a function of the initial relative density of the sands.

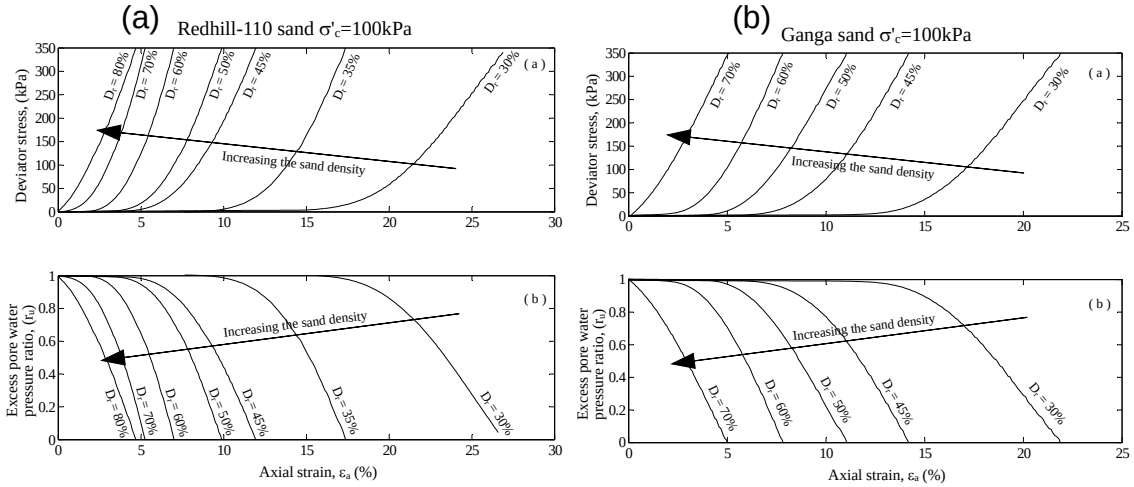

Figure 4: Typical post-liquefaction monotonic response for *CSR*=0.15 in Phase 1: (a) Redhill-110 sand; and (b) Ganga sand.

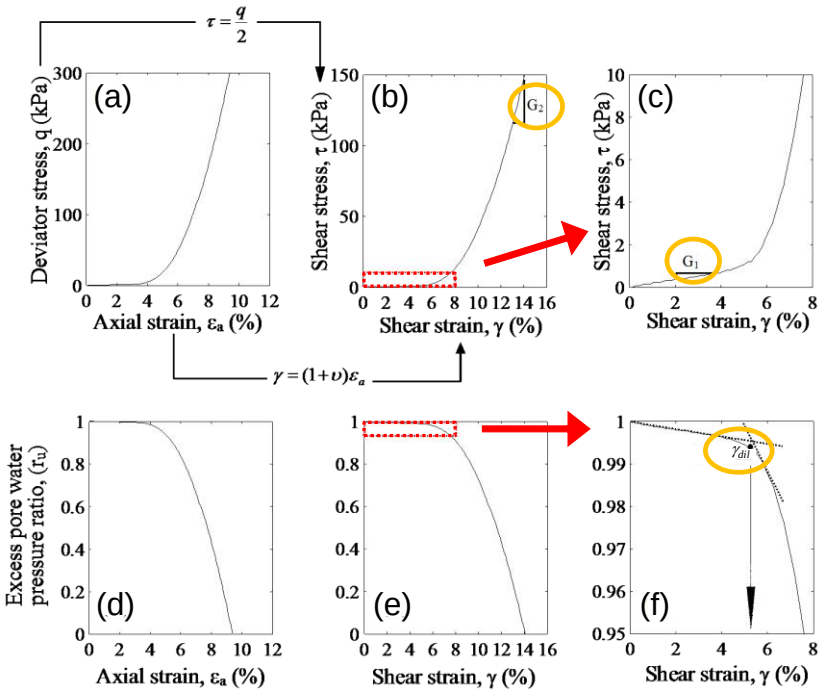

Figure 5: Schematic diagram showing the post-liquefaction stress-strain and excess pore water pressure ratio in normal and magnified situation: (a) axial strain vs deviator stress; (b) shear strain vs shear stress; (c) magnified shear strain-shear stress curve; (d) axial strain vs excess pore water pressure ratio; (e) shear strain vs excess pore water pressure ratio; and (f) magnified shear strain vs excess pore water pressure ratio.

Collating the values corresponding to the slopes G_1 and G_2, as well as the shear strain, γ_{dil}, for all the test results on four different sands, they are then correlated to the initial density of the specimen D_r; the results are shown in Figure 6. While there is a significant scatter, each of these parameters can be said to be a function of the relative density of the sands. Thus, if D_r of sand in-situ is estimated empirically (e.g. from penetration resistance or any other means), the three post-liquefaction parameters can be approximated and the post-liquefaction undrained response can be defined.

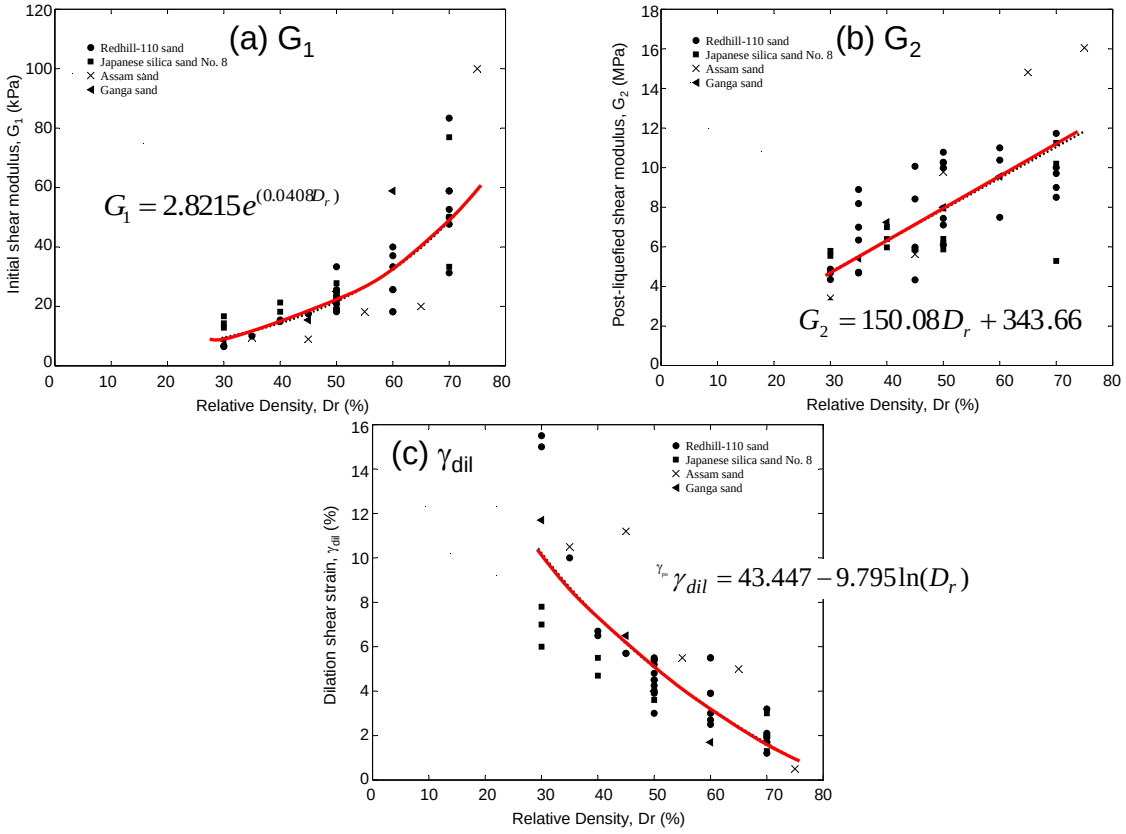

Figure 6: Variation of: (a) G_1; (b) G_2; and (c) γ_{dil} with respect to D_r for σ'_c=100 kPa.

3.2 Phase 2

A similar series of tests was performed on reconstituted natural pumiceous deposits and Toyoura sand. While it is obvious that the cyclic and post-cyclic response of Toyoura sand would be similar to those of the hard-grained sands used in Phase 1 and discussed above, the general behaviour of pumiceous sand appears to be relatively similar. A typical undrained behaviour (NP2 sample as a representative of the materials tested) is shown in Figure 7 for loose condition under σ'_c=100 kPa and *CSR*=0.22 when the soil was induced to liquefy (i.e. the attainment of 5% double amplitude axial strain). Application of monotonic load results in some deformation with almost zero stiffness; however, once a certain threshold strain is reached, the specimen dilates and the excess pore water pressure drops accompanied by an increase in shear stress.

While the general response of liquefied pumiceous sand to undrained loading is generally similar to that of liquefied Toyoura sand, detailed investigation showed subtle differences. Figure 8 illustrates the effect of relative density on the post-liquefaction behaviour of the two sands. Based on the results of several tests, the following are the main observations made:

- The post-liquefaction behaviour of Toyoura sand is affected more by D_r when compared to pumiceous sand;

- For similar D_r, the initial shear modulus, G_1, of pumiceous sand is higher while its shear modulus at recovery, G_2, is lower than those of Toyoura sand; and
- The region corresponding to negligible shear strength and, consequently, the magnitude of γ_{dil} are smaller for pumiceous sand, indicating that the pumiceous sand recovers its stiffness at considerably lower strain compared to Toyoura sand.

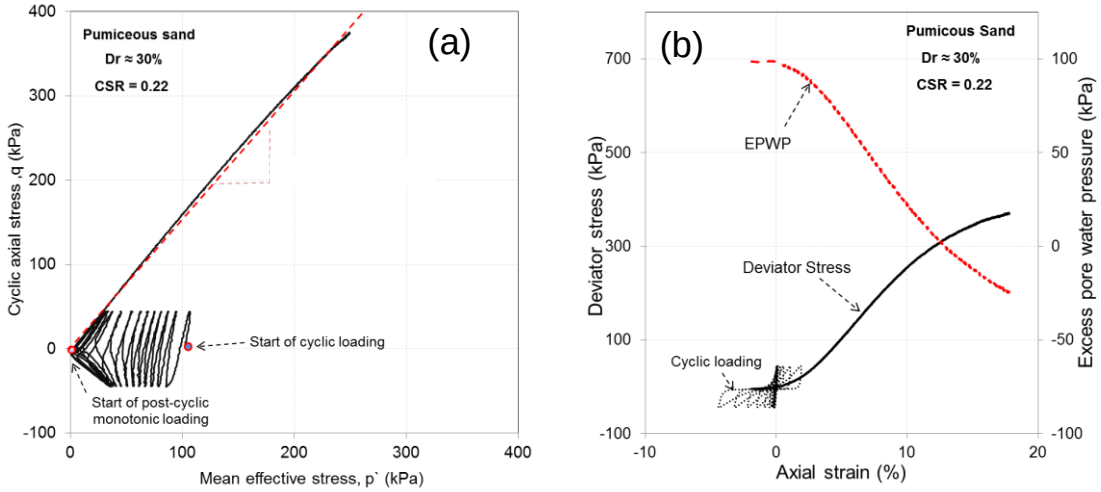

Figure 7: Typical response of loose (D_r≈30%) pumiceous sand (NP2): (a) effective stress path; (b) variation of deviator stress and EPWP with axial strain

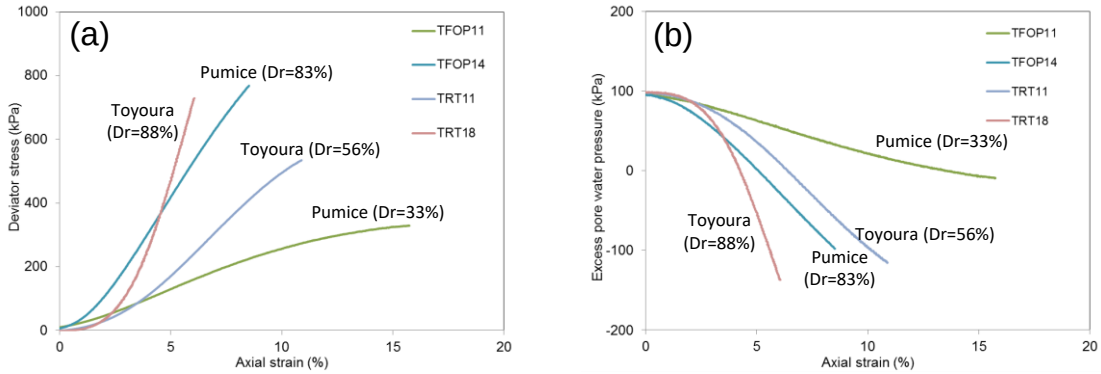

Figure 8: Comparison of the post-liquefaction undrained behaviour of Toyoura sand and NP2 pumiceous sand: (a) stress-strain relation; and (b) pore water pressure response.

The different behaviour of liquefied pumiceous and Toyoura sands under the application of monotonic loading may be attributed to the different ways by which the fabric changes during cyclic loading. Based on laboratory tests performed by Asadi et al. (2017), pumice particles are easily crushed during shearing; the crushing and the inherently high angularity of pumice particles, as observed through SEM image analyses, induce interlocking between them when sheared; thus, they recover their stiffness at considerably lower strain than Toyoura sand.

4 CONCLUDING REMARKS

The stress-strain behaviour of liquefied sand can be modelled as a bilinear curve which is defined in terms of three parameters: initial shear modulus (G_1); shear modulus at recovery (G_2); and dilation shear strain (γ_{dil}). Each of these parameters is a function of the initial relative density of the sand. Thus, if the in-situ relative density of sand is estimated empirically (e.g. from penetration resistance or any other means), the three post-liquefaction parameters can be approximated and the in-situ post-liquefaction undrained behaviour can be defined.

Crushable pumiceous sands appeared not to follow the behaviour of hard-grained sand. Previous research indicated that particle crushing occurred during cyclic and monotonic phases and this contributed to the formation of more stable soil skeleton and, coupled with the high angularity of the particles, induced interlocking during shearing.

5 ACKNOWLEDGEMENT

The Phase 1 research reported in this paper was based on work conducted while the first author was on Research & Study Leave at the University of Surrey, U.K. Phase 2 was done at the Geomechanics Laboratory, University of Auckland, with the help of M.B. Asadi. The authors would like to acknowledge the assistance of all those involved in both research.

REFERENCES

Asadi, M.S., Asadi, M.B., Orense, R.P., Pender, M.J., Jacobs, E. (2017). "Undrained cyclic and post-liquefaction behaviour of natural pumiceous soils," *3rd International Conference on Performance-based Design in Earthquake Geotechnical Engineering (PBD-III)*, Vancouver, BC, Canada, Paper 334, 7pp.

Hamada M. (1992) *Case Studies of Liquefaction and Lifeline Performance during Past Earthquakes, Vol. 1, Japanese Case Studies*, National Center for Earthquake Engineering Research, State Univ. of New York, Buffalo, N.Y.

Kokusho T, Hara T & Hiraoka R. (2004) Undrained shear strength of granular soils with different particle gradation. *J. Geotech. Eng. Div*., ASCE, 130(6), 621-629.

Hyodo M, Hyde AFL & Aramaki N. (1998) Liquefaction of crushable soils. *Geotechnique*, 48(4), 527-543.

Port and Harbour Research Institute (1997) *Handbook of Liquefaction Remediation in Reclaimed Lands*, Balkema.

Rouholamin M, Bhattacharya S & Orense R. (2017) Effect of initial relative density on the post-liquefaction behaviour of sand. *Soil Dynamics and Earthquake Engineering*, 97, 25-36.

Seed H B, Makdisi F, Idriss IM & Lee KL. (1975) The slides in the San Fernando Dams during the earthquake of February 9, 1971. *J. Geotech. Eng. Div*., ASCE, 101(7), 651-688.

Shamoto Y, Zhang JM & Goto S. (1997) Mechanism of large post-liquefaction deformation in saturated sand. *Soils and Foundations*, 37(2), 71-80.

Sitharam TG, Vinod JS & Ravishankar BV. (2009) Post-liquefaction undrained monotonic behaviour of sands: experiments and DEM simulations. *Geotechnique*, 59(9), 739-749.

Vaid Y & Thomas J. (1995) Liquefaction and post liquefaction behavior of sand. *J. Geotech. Eng. Div*., ASCE, 121(2), 163-173.

Yasuda S, Yoshida N, Masuda T, Nagase H, Mine K & Kiku H. (1995) Stress-strain relationships of liquefied sands. *International Conferences on Recent Advances in Geotechnical Earthquake Engineering and Soil Dynamics*, St. Louis, Missouri, 295-298.